European Journal of Radiology 115 (2019) 16–21

Contents lists available at ScienceDirect

European Journal of Radiology

journal homepage: www.elsevier.com/locate/ejrad

Research article

Multi-parametric MRI-based radiomics signature for discriminating between clinically significant and insignificant prostate cancer: Cross-validation of a machine learning method

Xiangde Min[a,1], Min Li[b,1], Di Dong[c,d,1], Zhaoyan Feng[a], Peipei Zhang[a], Zan Ke[a], Huijuan You[a], Fangfang Han[b], He Ma[b,**], Jie Tian[c,d,e,**], Liang Wang[a,*]

[a] Department of Radiology, Tongji Hospital, Tongji Medical College, Huazhong University of Science and Technology, Wuhan, Hubei Province, PR China
[b] Sino-Dutch Biomedical and Information Engineering School, Northeastern University, Shenyang, Liaoning Province, PR China
[c] CAS Key Laboratory of Molecular Imaging, Institute of Automation, Chinese Academy of Sciences, Beijing, PR China
[d] University of Chinese Academy of Sciences, Beijing, PR China
[e] Beijing Advanced Innovation Center for Big Data-Based Precision Medicine, School of Medicine, Beihang University, Beijing, PR China

ARTICLE INFO

Keywords:
Magnetic resonance imaging
Prostatic neoplasms
Neoplasm grading
Radiomics

ABSTRACT

Purpose: To evaluate the performance of a multi-parametric MRI (mp-MRI)-based radiomics signature for discriminating between clinically significant prostate cancer (csPCa) and insignificant PCa (ciPCa).

Materials and methods: Two hundred and eighty patients with pathology-proven PCa were enrolled and were randomly divided into training and test cohorts. Eight hundred and nineteen radiomics features were extracted from mp-MRI for each patient. The minority group in the training cohort was balanced via the synthetic minority over-sampling technique (SMOTE) method. We used minimum-redundancy maximum-relevance (mRMR) selection and the LASSO algorithm for feature selection and radiomics signature building. The classification performance of the radiomics signature for csPCa and ciPCa was evaluated by receiver operating characteristic curve analysis in the training and test cohorts.

Results: Nine features were selected for the radiomics signature building. Significant differences in the radiomics signature existed between the csPCa and ciPCa groups in both the training and test cohorts ($p < 0.01$ for both). The AUC, sensitivity and specificity of the radiomics signature were 0.872 (95% CI: 0.823 − 0.921), 0.883, and 0.753, respectively, in the training cohort, and 0.823 (95% CI: 0.669 − 0.976), 0.841, and 0.727, respectively, in the test cohort.

Conclusion: Mp-MRI-based radiomics signature have the potential to noninvasively discriminate between csPCa and ciPCa.

1. Introduction

Prostate cancer (PCa) is the second most frequently diagnosed male cancer worldwide [1]. Transrectal ultrasound (TRUS)-guided prostate biopsy is the routine diagnostic method in male patients who present with an elevated serum prostate-specific antigen (PSA). However, TRUS-guided biopsy may bring significant side effects, including bleeding, pain or infection. Some patients may undergo unnecessary biopsies because clinically insignificant PCa (ciPCa) may be detected. Moreover, the identification of ciPCa by TRUS-biopsy may result in overtreatment of some patients.

Multi-parametric MRI (mp-MRI) plays a crucial role in the management of PCa and has been suggested as a promising non-invasive imaging modality in the detection of PCa due to its functional and anatomical information [2]. Prebiopsy mp-MRI may predict the presence of csPCa, which could reduce the number of unnecessary biopsies for patients with ciPCa who are suspected of having PCa due to elevated PSA levels. Mp-MRI has high impact for both clinicians and patients to reduce the overdiagnosis and overtreatment of ciPCa and to schedule high-risk csPCa patients for biopsy or other treatment.

* Corresponding author at: Department of Radiology, Tongji Hospital, Tongji Medical College, Huazhong University of Science and Technology, No.1095 Jie Fang Avenue, Qiaokou, Wuhan 430030, PR China.
** Corresponding authors.
E-mail addresses: mahe@bmie.neu.edu.cn (H. Ma), jie.tian@ia.ac.cn (J. Tian), wang6@tjh.tjmu.edu.cn (L. Wang).
[1] These authors contributed equally to this work.

https://doi.org/10.1016/j.ejrad.2019.03.010
Received 7 November 2018; Received in revised form 13 March 2019; Accepted 14 March 2019

Radiomics is a new method of image analysis that can extract large amounts of quantitative and objective image features from radiologic images and select stable and clinically relevant radiomics biomarkers for disease evaluation. Many previous studies have suggested the great potentials of radiomics, especially in quantifying and monitoring tumour characteristics [3–10]. Radiomics had also been extended to the evaluation of PCa. However, the potential value of mp-MRI-based radiomics in predicting csPCa has not been fully investigated.

The purpose of our study was to investigate whether mp-MRI based radiomics could detect csPCa in patients with suspected PCa.

2. Materials and methods

2.1. Patients

This retrospective study was approved by the local review board. Between October 2013 and May 2017, consecutive patients who were pathology-proven to have PCa and received mp-MRI examination with the same MRI scanner prior to TRUS-guided systemic biopsy were included in this study. Patients were excluded for any of the following reasons: (a) patients with prior therapy including hormonal, irradiation, cryotherapy, or surgery; (b) poor quality of the MRI images due to movement artifacts, susceptibility artifacts or the presence of hip implants; (c) no visible lesion on mp-MRI images; (d) the clinical data, such as serum PSA level, were incomplete; (e) combined with other tumors and invaded to prostate tissue such as bladder cancer, rectal cancer. Ultimately, 280 patients were enrolled in this study. The included patients were randomly divided into training cohort (n = 187) and test cohort (n = 93). Patients' characteristics in the training and test cohorts are shown in Table 1. According to previous studies and prostate guideline, csPCa was defined as a Gleason score of 3 + 4 or higher in at least one biopsy core [2,11,12].

2.2. Pathological evaluation

All patients underwent both a TRUS-guided 12-core systematic biopsy and an MRI-targeted biopsy using the cognitive registration technique after the MRI examination. Cognitive-targeted biopsy had been suggested to be an effective method for PCa detection, and its accuracy for PCa detection is similar to that of MRI/ultrasound fusion biopsy [13,14]. The biopsy was performed by a single experienced urologist with 20 years of experience using an ultrasound system (Hawk 2102, BK Medical, Denmark). The dominant lesion suspicious for PCa was described according to its location, size, shape, and signal characteristics on MRI reports. The biopsy operator reviewed the MRI reports and attempted to specifically target the dominant lesions using cognitive registration. Cores were individually labelled according to their location. Each specimen was histologically analysed by an experienced pathologist who has over 15 years of experience.

2.3. MRI protocol

All examinations were performed with the same 3.0 T MRI scanner (Skyra, Siemens Healthcare, Erlangen, Germany), using an eighteen-channel abdomen coil above and a spine coil underneath the pelvis. The protocol included transverse T1-weighted turbo spin-echo sequence, axial, sagittal, and coronal T2-weighted turbo spin-echo sequence, and transverse diffusion weighted imaging (DWI). DWI was acquired with a minimum b-value of 0 s/mm^2 and maximum b-value of 1500s/mm^2. Apparent diffusion coefficient (ADC) maps were automatically reconstructed using a mono-exponential fit model from DWI images using the following formula:

$$S(b)/S_0 = \exp(-b \cdot ADC)$$

where S(b) is the signal intensity at a particular b-value, and S_0 is the signal intensity at b = 0 s/mm^2. ADC is the diffusion coefficient of the mono-exponential model. The detailed parameters of the MR sequences used are shown in Supplement S1.*2.4. MRI segmentation and radiomics feature extraction*

The ITK-SNAP software (version 3.4.0; www.itksnap.org) was used for manual segmentation. Preoperative transverse T2-weighted imaging (T2WI), ADC maps and DWI (b = 1500s/mm^2, DWI_{1500}) images were obtained for image analysis. The three-dimensional volume of interest (VOI) covering the dominant tumor was delineated by stacking regions of interest slice-by-slice on the ADC map and transverse T2WI on each slice. As the ADC maps were automatically reconstructed from DWI images, the ADC maps had the same locations as the DWI images. Therefore, the segmented VOIs were copied from the ADC maps to the DWI_{1500} images. Manual segmentation of the tumors on the images was performed initially by a radiologist. Then, all the segmentations were verified by a senior radiologist with 20 years of experience.

Feature extraction was completed using MATLAB software (version 2014a; MathWorks, Natick, MA). Three-dimensional features were extracted from transverse T2WI, DWI_{1500} and ADC sequences. The feature extraction method is described in detail in the Supplement S2.

2.4. Statistical analysis

The feature selection and radiomics signature construction process in the training cohort was performed using the following steps. The Mann-Whitney U test for non-normally distributed features or the independent *t*-test for normally distributed features was first performed to screen for significant features and redundant features, indicated by Spearman's correlation coefficient > 0.8, were eliminated [15]. Because class imbalance can influence the classification performance, the

Table 1
Characteristics of patients in the training and test cohorts.

Characteristics	Training cohort (n = 187)		Test cohort (n = 93)	
	CsPCa (n = 160)	CiPCa (n = 27)	CsPCa (n = 81)	CiPCa (n = 12)
Age (years)	68.8 ± 8.3	71.5 ± 8.4	70.3 ± 7.8	71.6 ± 5.7
PSA, No.				
≤4 ng/ml	1	1	0	1
4-10 ng/ml	15	5	4	5
> 10 ng/ml	124	10	71	6
Position, No.				
Peripheral zone	112	16	54	8
Transitional zone	48	11	27	4
Gleason score, No.				
6	None	27	None	12
7	55	None	22	None
8	58	None	31	None
≥9	47	None	28	None

synthetic minority over-sampling technique (SMOTE) was performed in the training cohort [16]. Then, the remaining features were ranked using the minimum-redundancy maximum -relevance (mRMR) algorithm by calculating the mutual information (MI) between features and csPCa. The mRMR ranks the input features by maximizing the MI with respect to the csPCa group and minimizing the average MI of higher ranked features. This technique allows an efficient selection of relevant and non-redundant features. In this study, only 10 of the highest-ranking features in mRMR selection were selected. The least absolute shrinkage and selection operator (LASSO) logistic regression model using 10-fold cross-validation was adopted for further feature selection. Features with non-zero coefficients were selected from the candidate features and were combined linearly to construct a radiomics signature [17].

To test the radiomics signature in a real experiment, SMOTE was not performed in the test cohort. The difference in radiomics signature between the csPCa and ciPCa groups were compared using the Mann-Whitney U test in the training and test cohorts. The predictive ability of the radiomics signature was evaluated using the receiver operating characteristic (ROC) curve. The area under the curve (AUC), sensitivity and specificity were derived in both the training and test cohorts. The framework for the radiomics workflow is shown in Fig. 1.

The statistical analyses were performed using R software (version 3.3.4; http://www.Rproject.org). The following R packages were used: the "corrplot" package was used to calculate Spearman's correlation coefficient; the "DMwR" package was used to perform the SMOTE algorithm; the "mRMRe" package was used to implement the mRMR algorithm; the "glmnet" was used to perform the LASSO logistic regression model; and the "pROC" package was used to construct the ROC curve. A two-sided p-value < 0.05 was taken to indicate statistical significance for all statistical analyses. To control the false positive rate in multiple comparisons, the false discovery rate adjusted p-value was used in the Mann-Whitney U test and the independent *t*-test during feature selection.

3. Results

A total of 273 quantitative features were extracted from the VOI of each of the MRI series and its corresponding filtered results. In the current study, 819 radiomics features for each patient were extracted from mp-MRI (T2WI, ADC and DWI_{1500}).

Eight insignificant features were eliminated first. After eliminating the redundant features using the threshold value of Spearman's correlation coefficient > 0.80, 93 features with low correlation remained. The correlation matrix heatmaps of features in the training cohort before and after correlation filtering are shown in Fig. 2. The selection result of the remaining features for mRMR selection is shown in Table 2. Through the 10-fold cross-validation of the LASSO algorithm, 9 features (three features from T2WI, 2 features from DWI and 4 features from ADC maps) with non-zero coefficients were included for radiomics signature construction. The process of feature selection using the LASSO algorithm is shown in Fig. 3. The calculation formula of the radiomics signature construction is shown in Table 3. The contribution of features to the radiomic signature is shown in Fig. 4.

There were significant differences in the radiomics signature between the csPCa and ciPCa groups in both the training and test cohorts ($p < 0.01$ for both). The ROC curves of the radiomics signature in discriminating csPCa from ciPCa in both the training and test cohorts are shown in Fig. 5. The AUC, sensitivity and specificity of the radiomics signature were 0.872 (95% CI: 0.823 – 0.9212), 0.883, and 0.753, respectively, in the training cohort, and 0.823 (95% CI: 0.669 – 0.976), 0.841, and 0.727, respectively, in test cohort.

4. Discussion

Noninvasively discriminating between csPCa and ciPCa is of great significance. Providing both functional and anatomical information, mp-MRI has been applied for the prediction of csPCa in many studies. In this study, we adopted advanced radiomics to prostate MRI for the prediction of csPCa. A mp-MRI-based radiomics signature for discriminating between csPCa and ciPCa was constructed and tested.

While the current PSA-and-biopsy based diagnosis has reduced mortality associated with PCa, some ciPCa may be overdiagnosed. Previous studies estimated that approximately 40% of the positive screening cases and more than 3% of the screening cases may experience overdiagnosis of PCa [18,19]. Overdiagnosis of ciPCa would lead to overtreatment [20], which may introduce the side-effects of aggressive treatment (e.g. erectile dysfunction and urinary incontinence). Noninvasively, prebiopsy discriminating csPCa from ciPCa may reduce unnecessary biopsies and minimize overdiagnosis/overtreatment of ciPCa. The possibility of side-effects and overdiagnosis associated with PSA-and-biopsy based diagnosis warrants new effective and non-invasive methods for prediction of csPCa and ciPCa.

Providing a large amount of anatomical and functional information, mp-MRI is a promising method for the non-invasive evaluation of PCa. Many previous studies have evaluated the performance of mp-MRI-based models for prediction csPCa [11,21–24]. Yim JH et al. combined Prostate Imaging Reporting and Data System scores and the tumour

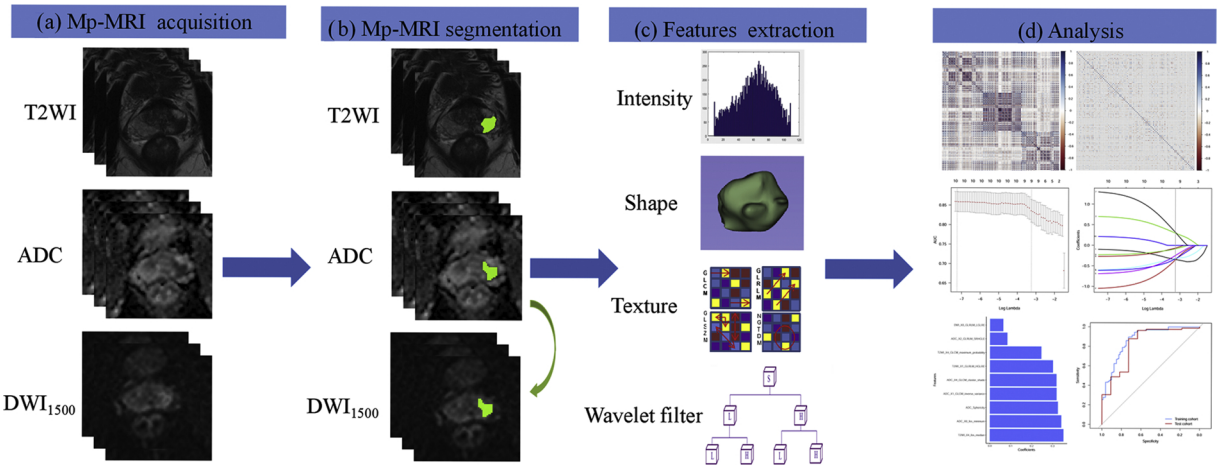

Fig. 1. The framework for the radiomics workflow. (a) Patient scanned with preoperative mp-MRI. (b) The dominate tumor was delineated by stacking up regions of interest slice-by-slice on the ADC map and transverse T2WI image on each slice. The segmented volume of interest was copied from ADC maps to DWI_{1500} images. (c) High-throughput radiomics features were extracted from mp-MRI. (d) Data analysis for feature selection, radiomics signature construction and testing.

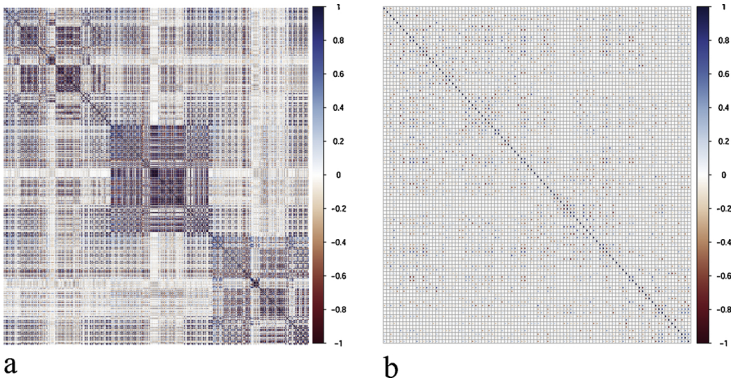

Fig. 2. Correlation matrix heatmaps of features in the training cohort before (a) and after (b) correlation filtering. Before correlation filtering, a mass of redundant features with high correlation coefficients existed.

Table 2
Features selected from mRMR.

Features	mRMR scores	Groups	Filters
ADC_X0_fos_minimum	0.131979	First-order statistics feature	NA
T2WI_X4_fos_median	0.036235	Wavelet feature	X_{LH}
T2WI_X1_GLRLM_HGLRE	0.013669	Wavelet feature	X_{LL}
ADC_Sphericity	0.022909	Shape-and size-based feature	NA
ADC_X4_GLCM_cluster_shade	0.038574	Wavelet feature	X_{LH}
T2WI_X4_GLCM_maximum_probability	0.021016	Wavelet feature	X_{LH}
ADC_X1_GLCM_inverse_variance	0.019298	Wavelet feature	X_{LL}
DWI_X0_GLRLM_LGLRE	0.010225	Statistics-based textural feature	NA
ADC_X2_GLRLM_SRHGLE	0.013616	Wavelet feature	X_{HL}
DWI_X2_GLCM_cluster_tendency	0.003729	Wavelet feature	X_{HL}

NOTE. mRMR: minimum-redundancy maximum-relevance; ADC: apparent diffusion coefficient; T2WI: T2-weighted imaging; fos: first-order statistics features; GLRLM: gray-level run-length texture matrix; GLCM: grey-level co-occurrence matrix; NA: not applicable.

Table 3
Calculation formula for radiomics signature.

Variables	Coefficients
Intercept	0.77495115
ADC_X0_fos_minimum	0.34119165
T2WI_X4_fos_median	0.35146236
T2WI_X1_GLRLM_HGLRE	0.30077846
ADC_Sphericity	0.32456821
ADC_X4_GLCM_cluster_shade	0.31770603
T2WI_X4_GLCM_maximum_probability	0.24512478
ADC_X1_GLCM_inverse_variance	0.31825114
DWI_X0_GLRLM_LGLRE	0.0630764
ADC_X2_GLRLM_SRHGLE	0.08281175

NOTE. ADC: apparent diffusion coefficient; T2WI: T2-weighted imaging; fos: first-order statistics features; GLRLM: gray-level run-length texture matrix; GLCM: grey-level co-occurrence matrix.

ADC value reaching an AUC of 0.803 for predicting patients with ciPCa [21]. In another study by Pim J. van et al., they established a mp-MRI-based prediction model for csPCa detection [24]. The AUC of the advanced model in predicting csPCa was 0.88. In a recent study by Costa ND et al., the mean ADC values were explored for discriminating between csPCa and ciPCa. The AUC for the peripheral zone PCa was 0.91, and the AUC for the transition zone PCa was 0.70. Although some positive results for the MRI-based classifier in distinguishing csPCa from ciPCa have been reported, most previous studies included limited MRI features that may not fully explore potential information. Contrary to the above studies, a large amount of quantitative features were included in our study, and the most effective features were selected for the construction of the prediction model. In current study, a total of 819 radiomics features from mp-MRI images were extracted.

The newly proposed radiomics method has been successfully applied in many diseases and has been extended to PCa detection and evaluation [25–27]. A previous study by Algohary et al. evaluated the performance of mp-MRI based radiomics features in identifying the presence or absence of csPCa [26]. Their results suggested a role for mp-MRI-based radiomics features in predicting the presence of csPCa. In contrast to the study by Algohary et al., our study focused on distinguishing between csPCa and ciPCa rather than malignant and normal

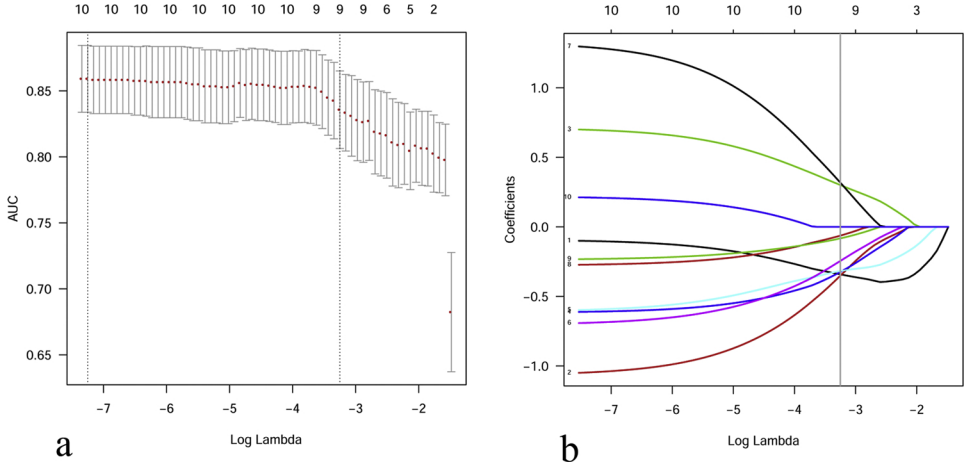

Fig. 3. Feature selection using the LASSO algorithm. (a) The optimal tuning parameter (Lambda) in the LASSO model was selected using 10-fold cross-validation and the 1 standard error rule. The optimal Lambda value of 0.0388 with log (Lambda) =-3.249 and 9 nonzero coefficients were chosen; (b) LASSO coefficient profiles of the 10 features. According to the 10-fold cross-validation in (a), the vertical line was drawn. The 9 features with non-zero coefficients were included for radiomics signature construction.

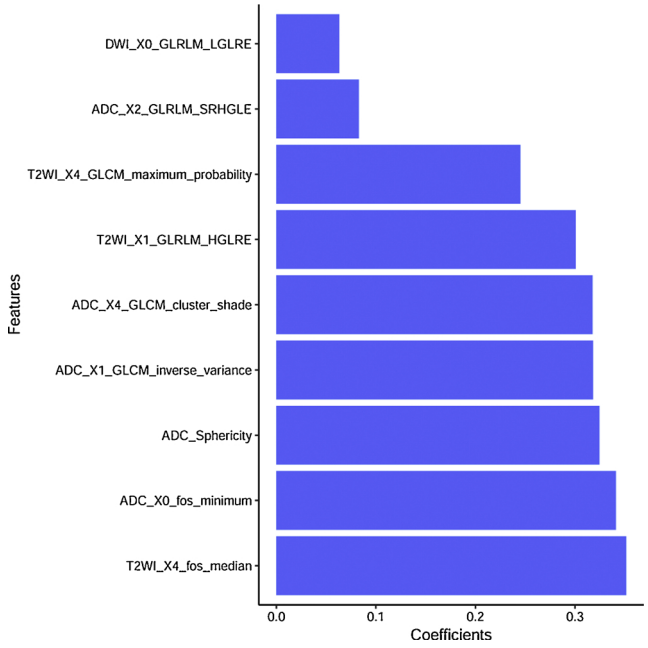

Fig. 4. Histogram showing contribution of each feature to the radiomic signature.

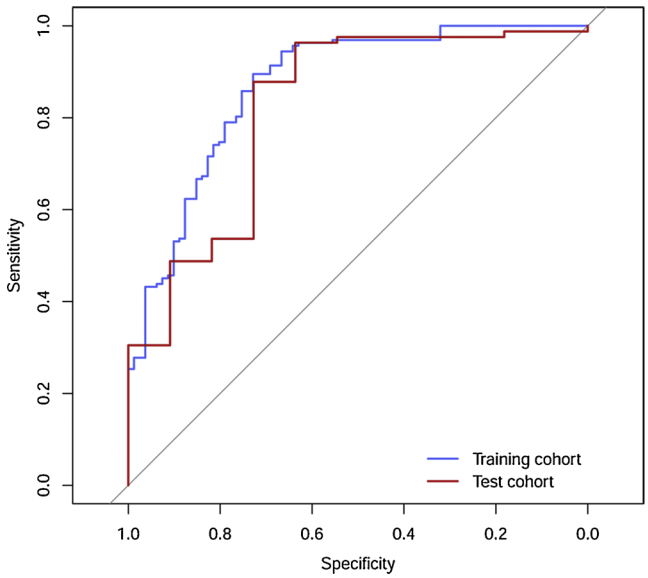

Fig. 5. ROC curves of the radiomics signature in the training (a) and test (b) cohorts. The AUCs in the training and test cohorts were 0.872 (95% CI: 0.823 – 0.9212) and 0.823 (95% CI: 0.669 – 0.976), respectively.

prostate regions. Another study by Shiradkar et al. explored the radiomics features from bi-parametric MRI in predicting the biochemical recurrence of PCa [27]. Their results illustrated that radiomics features from pretreatment bi-parametric MRI can be used to predict biochemical recurrence of PCa after therapy and may help identify patients who would benefit from adjuvant therapy. Radiomics has shown great potential value for the diagnosis and evaluation of PCa. However, no study has fully evaluated the potential value of mp-MRI-based radiomics signature in predicting csPCa. In this study, we extracted high-throughput imaging features from mp-MRI and constructed a mp-MRI-based radiomics signature for the prediction of csPCa. The result of this study provides a new mp-MRI tool for discriminating between csPCa and ciPCa. Our results showed that the radiomics signature provides relatively high efficiency for discriminating csPCa and ciPCa in both training and test cohorts (AUC = 0.872 and 0.823, respectively). The sensitivity and specificity of the radiomics signature for prediction csPCa were 0.841and 0.727, respectively, in the test cohort.

There are usually inter-group imbalances in medical data. This imbalance could cause significant bias for the constructed radiomics signature in the training process and would also affect the prediction performance of the radiomics signature in the testing process. In the current study, the proportion of the csPCa and ciPCa is significantly imbalanced (160 vs 27). To alleviate the effect of the imbalance in the training cohort, we adopted the powerful and effective SMOTE algorithm in the training cohort. However, the SMOTE algorithm was not performed in the test cohort because we wanted to test the radiomics signature in a real experiment. Another aspect that should be pointed out is the quality assurance for MRI scanner. The current data were gathered over a time period of approximately 3.5 years; therefore, the quality assurance for the MRI scanner was important for this long-duration study. In our situation, the after-sale service department of Siemens Healthineers regularly provided specialized quality assurance for the MRI scanner used in the current study.

There are some limitations in this study. First, this is a retrospective study from a single centre. Further data from multiple centres are needed to validate our primary results. Second, systematic biopsy and cognitive-targeted biopsy were used as the reference standard rather than whole-mount serial section. The use of whole-mount histopathology improves the accuracy of the agreement between MR images and histopathology. However, it is unreasonable to expect that all of our subjects would undergo prostatectomy, especially for ciPCa patients. Additionally, only including patients who underwent prostatectomy would also introduce selection bias. Third, patients with no visible lesions on mp-MRI were excluded in current study. This is because we could not delineate the tumour region during MRI segmentation for these patients. Therefore, some selection bias may be introduced. Despite the limitations of our study, we believe that our methodical strategies provide sufficient validity for the principal results of our primary study.

In conclusion, a mp-MRI-based radiomics signature for discriminating csPCa from ciPCa was constructed and validated in present study. The radiomics signature from mp-MRI provided a non-invasive and quantitative method. Further studies are warranted to validate our primary results. This radiomics signature may help clinicians facilitate prebiopsy and pre-treatment risk stratification.

Conflicts of interest

None.

Acknowledgements

This work was supported by the National Natural Science Foundation of China (81671656, 81801668, 81771924, 81501616, 81227901, and81671854), the Beijing Natural Science Foundation (L182061), National Key R&D Program of China (2017YFA0205200, 2017YFC1308700, 2017YFC1308701, 2017YFC1309100, 2016YFC0103803), the Science and Technology Service Network Initiative of the Chinese Academy of Sciences (KFJ-SW-STS-160), the Beijing Municipal Science and Technology Commission (Z171100000117023, Z161100002616022), and the Youth Innovation Promotion Association CAS.

Appendix A. Supplementary data

Supplementary material related to this article can be found, in the online version, at doi:https://doi.org/10.1016/j.ejrad.2019.03.010.

References

[1] F. Bray, J. Ferlay, I. Soerjomataram, R.L. Siegel, L.A. Torre, A. Jemal, Global cancer statistics 2018: GLOBOCAN estimates of incidence and mortality worldwide for 36 cancers in 185 countries, CA Cancer J. Clin. 68 (6) (2018) 394–424.

[2] J.C. Weinreb, J.O. Barentsz, P.L. Choyke, F. Cornud, M.A. Haider, K.J. Macura, D. Margolis, M.D. Schnall, F. Shtern, C.M. Tempany, H.C. Thoeny, S. Verma, PI-RADS Prostate Imaging - Reporting and Data System: 2015, Version 2, Eur. Urol. 69 (1) (2016) 16–40.

[3] K. Wang, X. Lu, H. Zhou, Y. Gao, J. Zheng, M. Tong, C. Wu, C. Liu, L. Huang, T. Jiang, F. Meng, Y. Lu, H. Ai, X.Y. Xie, L.P. Yin, P. Liang, J. Tian, R. Zheng, Deep learning radiomics of shear wave elastography significantly improved diagnostic performance for assessing liver fibrosis in chronic hepatitis B: a prospective multicentre study, Gut 68 (4) (2019) 729–741.

[4] D. Dong, L. Tang, Z.Y. Li, M.J. Fang, J.B. Gao, X.H. Shan, X.J. Ying, Y.S. Sun, J. Fu, X.X. Wang, L.M. Li, Z.H. Li, D.F. Zhang, Y. Zhang, Z.M. Li, F. Shan, Z.D. Bu, J. Tian, J.F. Ji, Development and validation of an individualized nomogram to identify occult peritoneal metastasis in patients with advanced gastric cancer, Ann. Oncol. 30 (3) (2019) 431–438.

[5] S. Bickelhaupt, P.F. Jaeger, F.B. Laun, W. Lederer, H. Daniel, T.A. Kuder, L. Wuesthof, D. Paech, D. Bonekamp, A. Radbruch, S. Delorme, H.P. Schlemmer, F.H. Steudle, K.H. Maier-Hein, Radiomics based on adapted diffusion kurtosis imaging helps to clarify most mammographic findings suspicious for cancer, Radiology 287 (3) (2018) 761–770.

[6] P. Lambin, R.T.H. Leijenaar, T.M. Deist, J. Peerlings, E.E.C. de Jong, J. van Timmeren, S. Sanduleanu, R. Larue, A.J.G. Even, A. Jochems, Y. van Wijk, H. Woodruff, J. van Soest, T. Lustberg, E. Roelofs, W. van Elmpt, A. Dekker, F.M. Mottaghy, J.E. Wildberger, S. Walsh, Radiomics: the bridge between medical imaging and personalized medicine, Nat. Rev. Clin. Oncol. 14 (12) (2017) 749–762.

[7] H. Li, Y. Zhu, E.S. Burnside, K. Drukker, K.A. Hoadley, C. Fan, S.D. Conzen, G.J. Whitman, E.J. Sutton, J.M. Net, M. Ganott, E. Huang, E.A. Morris, C.M. Perou, Y. Ji, M.L. Giger, MR imaging radiomics signatures for predicting the risk of breast cancer recurrence as given by research versions of MammaPrint, oncotype DX, and PAM50 gene assays, Radiology 281 (2) (2016) 382–391.

[8] Y.Q. Huang, C.H. Liang, L. He, J. Tian, C.S. Liang, X. Chen, Z.L. Ma, Z.Y. Liu, Development and validation of a radiomics nomogram for preoperative prediction of lymph node metastasis in colorectal cancer, J. Clin. Oncol. 34 (18) (2016) 2157–2164.

[9] H.J. Aerts, E.R. Velazquez, R.T. Leijenaar, C. Parmar, P. Grossmann, S. Carvalho, J. Bussink, R. Monshouwer, B. Haibe-Kains, D. Rietveld, F. Hoebers, M.M. Rietbergen, C.R. Leemans, A. Dekker, J. Quackenbush, R.J. Gillies, P. Lambin, Decoding tumour phenotype by noninvasive imaging using a quantitative radiomics approach, Nat. Commun. 5 (2014) 4006.

[10] P. Lambin, E. Rios-Velazquez, R. Leijenaar, S. Carvalho, R.G. van Stiphout, P. Granton, C.M. Zegers, R. Gillies, R. Boellard, A. Dekker, H.J. Aerts, Radiomics: extracting more information from medical images using advanced feature analysis, Eur. J. Cancer 48 (4) (2012) 441–446.

[11] S. Mehralivand, J.H. Shih, S. Rais-Bahrami, A. Oto, S. Bednarova, J.W. Nix, J.V. Thomas, J.B. Gordetsky, S. Gaur, S.A. Harmon, M.M. Siddiqui, M.J. Merino, H.L. Parnes, B.J. Wood, P.A. Pinto, P.L. Choyke, B. Turkbey, A Magnetic Resonance Imaging-based Prediction Model for Prostate Biopsy Risk Stratification, JAMA Oncol. 4 (5) (2018) 678–685.

[12] D. Hausmann, N. Aksoz, J. von Hardenberg, T. Martini, N. Westhoff, S. Buettner, S.O. Schoenberg, P. Riffel, Prostate cancer detection among readers with different degree of experience using ultra-high b-value diffusion-weighted imaging: Is a non-contrast protocol sufficient to detect significant cancer? Eur. Radiol. 28 (2) (2018) 869–876.

[13] J. Haffner, L. Lemaitre, P. Puech, G.P. Haber, X. Leroy, J.S. Jones, A. Villers, Role of magnetic resonance imaging before initial biopsy: comparison of magnetic resonance imaging-targeted and systematic biopsy for significant prostate cancer detection, BJU Int. 108 (8 Pt 2) (2011) E171–8.

[14] J.S. Wysock, A.B. Rosenkrantz, W.C. Huang, M.D. Stifelman, H. Lepor, F.M. Deng, J. Melamed, S.S. Taneja, A prospective, blinded comparison of magnetic resonance (MR) imaging-ultrasound fusion and visual estimation in the performance of MR-targeted prostate biopsy: the PROFUS trial, Eur. Urol. 66 (2) (2014) 343–351.

[15] W. Wu, C. Parmar, P. Grossmann, J. Quackenbush, P. Lambin, J. Bussink, R. Mak, H.J. Aerts, Exploratory study to identify radiomics classifiers for lung cancer histology, Front. Oncol. 6 (2016) 71.

[16] A.E. Fetit, J. Novak, D. Rodriguez, D.P. Auer, C.A. Clark, R.G. Grundy, A.C. Peet, T.N. Arvanitis, Radiomics in paediatric neuro-oncology: a multicentre study on MRI texture analysis, NMR Biomed. 31 (1) (2018).

[17] J. Shu, Y. Tang, J. Cui, R. Yang, X. Meng, Z. Cai, J. Zhang, W. Xu, D. Wen, H. Yin, Clear cell renal cell carcinoma: CT-based radiomics features for the prediction of Fuhrman grade, Eur. J. Radiol. 109 (2018) 8–12.

[18] G. Draisma, R. Etzioni, A. Tsodikov, A. Mariotto, E. Wever, R. Gulati, E. Feuer, H. de Koning, Lead time and overdiagnosis in prostate-specific antigen screening: importance of methods and context, J. Natl. Cancer Inst. 101 (6) (2009) 374–383.

[19] G.H. Wu, A. Auvinen, L. Maattanen, T.L. Tammela, U.H. Stenman, M. Hakama, A.M. Yen, H.H. Chen, Number of screens for overdetection as an indicator of absolute risk of overdiagnosis in prostate cancer screening, Int. J. Cancer 131 (6) (2012) 1367–1375.

[20] S. Loeb, M.A. Bjurlin, J. Nicholson, T.L. Tammela, D.F. Penson, H.B. Carter, P. Carroll, R. Etzioni, Overdiagnosis and overtreatment of prostate cancer, Eur. Urol. 65 (6) (2014) 1046–1055.

[21] J.H. Yim, C.K. Kim, J.H. Kim, Clinically insignificant prostate cancer suitable for active surveillance according to prostate cancer research International: active surveillance criteria: utility of PI-RADS v2, J. Magn. Reson. Imaging 47 (4) (2018) 1072–1079.

[22] M. Taghipour, A. Ziaei, F. Alessandrino, E. Hassanzadeh, M. Harisinghani, M. Vangel, C.M. Tempany, F.M. Fennessy, Investigating the role of DCE-MRI, over T2 and DWI, in accurate PI-RADS v2 assessment of clinically significant peripheral zone prostate lesions as defined at radical prostatectomy, Abdom. Radiol. (NY) 44 (4) (2019) 1520–1527.

[23] L.J. Bains, U.E. Studer, J.M. Froehlich, G. Giannarini, M. Triantafyllou, A. Fleischmann, H.C. Thoeny, Diffusion-weighted magnetic resonance imaging detects significant prostate cancer with high probability, J. Urol. 192 (3) (2014) 737–742.

[24] P.J. van Leeuwen, A. Hayen, J.E. Thompson, D. Moses, R. Shnier, M. Bohm, M. Abuodha, A.M. Haynes, F. Ting, J. Barentsz, M. Roobol, J. Vass, K. Rasiah, W. Delprado, P.D. Stricker, A multiparametric magnetic resonance imaging-based risk model to determine the risk of significant prostate cancer prior to biopsy, BJU Int. 120 (6) (2017) 774–781.

[25] S.B. Ginsburg, A. Algohary, S. Pahwa, V. Gulani, L. Ponsky, H.J. Aronen, P.J. Bostrom, M. Bohm, A.M. Haynes, P. Brenner, W. Delprado, J. Thompson, M. Pulbrock, P. Taimen, R. Villani, P. Stricker, A.R. Rastinehad, I. Jambor, A. Madabhushi, Radiomic features for prostate cancer detection on MRI differ between the transition and peripheral zones: preliminary findings from a multi-institutional study, J. Magn. Reson. Imaging 46 (1) (2017) 184–193.

[26] A. Algohary, S. Viswanath, R. Shiradkar, S. Ghose, S. Pahwa, D. Moses, I. Jambor, R. Shnier, M. Bohm, A.M. Haynes, P. Brenner, W. Delprado, J. Thompson, M. Pulbrock, A.S. Purysko, S. Verma, L. Ponsky, P. Stricker, A. Madabhushi, Radiomic features on MRI enable risk categorization of prostate cancer patients on active surveillance: preliminary findings, J. Magn. Reson. Imaging 48 (3) (2018) 818–828.

[27] R. Shiradkar, S. Ghose, I. Jambor, P. Taimen, O. Ettala, A.S. Purysko, A. Madabhushi, Radiomic features from pretreatment biparametric MRI predict prostate cancer biochemical recurrence: preliminary findings, J. Magn. Reson. Imaging 48 (6) (2018) 1626–1636.